

# Two component dark matter with multi-Higgs portals

---

Ligong Bian,<sup>a,1</sup> Tianjun Li,<sup>a,b</sup> Jing Shu,<sup>a</sup> and Xiao-Chuan Wang,<sup>a</sup>

<sup>a</sup>*State Key Laboratory of Theoretical Physics and Kavli Institute for Theoretical Physics China, Institute of Theoretical Physics, Chinese Academy of Sciences, Beijing 100190, P. R. China*

<sup>b</sup>*School of Physical Electronics, University of Electronic Science and Technology of China, Chengdu 610054, P. R. China*

*E-mail:* [lgb@itp.ac.cn](mailto:lgb@itp.ac.cn), [tli@itp.ac.cn](mailto:tli@itp.ac.cn), [jshu@itp.ac.cn](mailto:jshu@itp.ac.cn), [xcwang@itp.ac.cn](mailto:xcwang@itp.ac.cn)

## ABSTRACT:

With the assistance of two extra groups, i.e., an extra hidden gauge group  $SU(2)_D$  and a global  $U(1)$  group, we propose a two component dark matter (DM) model. After the symmetry  $SU(2)_D \times U(1)$  being broken, we obtain both the vector and scalar DM candidates. The two DM candidates communicate with the standard model (SM) via three Higgs as multi-Higgs portals. The three Higgs are mixing states of the SM Higgs, the Higgs of the hidden sector and real part of a supplement complex scalar singlet. We study relic density and direct detection of DM in three scenarios. The resonance behaviors and interplay between the two component DM candidates are represented through investigating of the relic density in the parameter spaces of the two DMs masses. The electroweak precision parameters constrains the two Higgs portals couplings ( $\lambda_m$  and  $\delta_2$ ). The relevant vacuum stability and naturalness problem in the parameter space of  $\lambda_m$  and  $\delta_2$  are studied as well. The model could alleviate these two problems in some parameter spaces under the constraints of electroweak precision observables and Higgs indirect search.

---

<sup>1</sup>Corresponding author.

---

## Contents

<b>1</b>	<b>Introduction</b>	<b>1</b>
<b>2</b>	<b>The Model</b>	<b>3</b>
<b>3</b>	<b>Dark matter analysis</b>	<b>5</b>
3.1	Relic density analysis	6
3.2	Direct detection	10
<b>4</b>	<b>Higgs indirect search and electroweak precision constraints</b>	<b>13</b>
4.1	Higgs indirect search	13
4.2	Electroweak precision observables constraints	13
<b>5</b>	<b>Vacuum stability</b>	<b>15</b>
<b>6</b>	<b>Footprint of the naturalness problem</b>	<b>16</b>
6.1	The naturalness problem	17
6.2	Indirect search for the scenario which alleviates the naturalness problem	18
<b>7</b>	<b>Discussions and conclusion</b>	<b>19</b>
<b>A</b>	<b>Annihilation Cross Sections</b>	<b>20</b>
<b>B</b>	<b>Boltzman equations</b>	<b>22</b>
<b>C</b>	<b>One loop <math>\beta</math> functions</b>	<b>23</b>

---

## 1 Introduction

The discovery of Higgs particle with mass around 126 GeV at Large hadron collider (LHC) [1, 2], roughly consistent with the SM predictions, seems complete the SM. However, the naturalness problem is still unsolved. To alleviate the problem, as well known and extensively studied, more bosonic fields are needed [3–7]. Recently, it has been noticed that the Higgs field-strength renormalization could be enhanced by these new boson fields [8–10]. And

that after the Higgs field normalization, the Higgs coupling's modification could be detected indirectly [9, 11]. Thus, it shed light on testing the mechanisms which alleviates the naturalness problem. Secondly, the SM has to be extended in order to accommodate the cold dark matter (CDM) and baryon number asymmetry of the universe (BAU). In order that the BAU not being washed out after its generation, the strong first order electroweak phase transition (SFOEWPT) is necessary, which is out of the capacity of the SM and new scalar fields are needed [12–14]<sup>1</sup>. At the same time, the way to test the mechanism alleviating the naturalness problem could also been used to test SFOEWPT, which is just one of the preliminary aims of the International Linear Collider (ILC) [8]. Thirdly, vacuum instability could be rescued by introducing vector and scalar fields [3, 17–22], and thus making the inflation with not very small top quark mass possible to coincide with the BICEP and Planck data [23, 24].

All above arguments require us to extend the SM with new bosonic freedoms, which we choose vector and scalar fields. There are many studies on the multi-component DM scenarios, see [3, 25–35], as well as the dynamical DM scenario [36] whose phenomenological consequences are often quite distinct and can be applied to a much broader variety of multi-component DM scenarios [37]. The primary purpose of this work is to explain the CDM relic density, where the two different DM components interact with each other besides with the three Higgses, thus affects the evolution of the DM components number densities through the coupled Boltzman equations [3, 38].

For the method to introduce vector dark matter through the effective Lagrangian method yielding strongly constraints on the parameters space from the unitarity constraints [3, 39, 40], we consider the scenario in which the vector dark matter fields ( $V^\mu$ ) respects an extra non-Abelian gauge symmetry  $SU(2)_D$ . After the  $SU(2)_D$  being broken via the the complex doublet( $\phi$ ), one  $SO(3)$  symmetry is induced which  $V^\mu$  respects to, thus making  $V^\mu$  stable.<sup>2</sup> One more complex scalar singlet,  $\mathbb{S}$ , is supplemented to the model. After the global  $U(1)$  symmetry, i.e.,  $\mathbb{S} \rightarrow e^{i\alpha}\mathbb{S}$  respected by  $V(H, \phi, \mathbb{S})$ , being broken spontaneously and softly, the real part of  $\mathbb{S}$  ( $S$ ) gets a vacuum expectation value(VEV), and the imaginary part of  $\mathbb{S}$  ( $A$ ) respects the reduced  $Z_2$  symmetry, which makes the other DM candidate. After the breaking of the  $SU(2)_D \times U(1)$ , the Higgs field of the SM mixed with two scalar fields, the real parts of  $\phi$  ( $\eta'$ ) and  $S$ . Since the two component DMs interact with the SM particles and each other through the three Higgs fields, one could expect three resonance enhancement effects. And three significant enlargement of the magnitude of the annihilation cross sections, of the DM to DM and the DM to SM particles, appears. The magnitudes of the relic density around the three resonances decrease, since which is robustly inversely proportional to the annihilation cross sections of the DM to SM particles. The magnitudes of annihilation cross sections of scalar DM fields (vector DM fields) to the SM particles, around the three Higgs field masses, are enlarged due to the  $t, u$  and seagull

---

<sup>1</sup> In fact, additional heavy fermions could also make the SFOEWPT feasible, see [15, 16].

<sup>2</sup>The hidden gauge theory has also been used to study self-interacting dark matter [42, 43], inflation [44], and the model with a kinetic mixing portal between the gauge boson DM and SM [41].

channels of  $AA(VV) \rightarrow h_i h_i$ <sup>3</sup>. The spin-independent (SI) DM-nucleon scattering cross sections are determined by  $t$ -channel interactions between the nucleon and two component DMs through the exchange of three Higgs fields. The model could be distinguished from the model with no interaction between the two DMs, since the opening of the channel  $AA \rightarrow VV(VV \rightarrow AA)$  does affect the evolution of DM number density, and thus the magnitude of relic density. This kind of effects are explored and illustrated in DM relic density analysis section of this work. The Higgs indirect search at the LHC requires small mixing between  $h$  and  $\eta'$  ( $S$ ). The electroweak precision observable experiment imposes stringent constraints on our parameter spaces. The vacuum stability of the model could be improved under the above two considerations. We explored the way to alleviate the naturalness problem and its' indirect search as well.

The paper is organized as follows. We construct the model and explore relic density and direct detection of the DMs. After which, we investigate the Higgs indirect search and electroweak precision constraints on the model. And then the stability of the model are studied. We also consider the possibility to alleviate naturalness problem and the way to trace the footprint of which. At last, we conclude this work with discussions and conclusion.

## 2 The Model

To construct the model which includes the stable vector and scalar fields, we introduce these two fields as follows. The vector field  $V'^\mu$  is introduced as the gauged field of the  $SU(2)_D$  symmetry, which couples to the SM through a doublet,  $\phi$ , which is a singlet of the SM but charged under the  $SU(2)_D$ . Here, one should note that the mixing between  $V'^\mu$  and the SM gauge bosons through kinetic mixing is absent for the non-abelian character of the  $SU(2)_D$ . We supplement one more complex singlet  $\mathbb{S}$ . And one more global  $U(1)$  symmetry is required besides the  $SU(2)_D$  and the SM group. The complex singlet, which interacts with the SM and the  $SU(2)_D$  through the Higgs portal and  $\phi$  portal terms in the scalar potential, transforms trivially under the SM and  $SU(2)_D$  gauge group.

The Lagrangian of our model is

$$\begin{aligned} \mathcal{L} = & \mathcal{L}^{SM} - \frac{1}{4} F'^{\mu\nu} \cdot F'_{\mu\nu} + (D_\mu \phi)^\dagger (D^\mu \phi) - \frac{\mu_\phi^2}{2} \phi^\dagger \phi - \frac{\lambda_\phi}{4} (\phi^\dagger \phi)^2 \\ & + \frac{b_2}{2} |\mathbb{S}|^2 + \frac{d_2}{4} |\mathbb{S}|^4 + \left( \frac{1}{4} b_1 e^{i\phi b_1} \mathbb{S}^2 + a_1 e^{i\phi a_1} \mathbb{S} + \text{c.c.} \right) \\ & + V_{H,\phi,\mathbb{S}} , \end{aligned} \tag{2.1}$$

with

$$V_{H,\phi,\mathbb{S}} = V_{H,\phi} + V_{H,S} + V_{\phi,S} , \tag{2.2}$$

---

<sup>3</sup>Hereafter, the Lorenz index  $\mu$  of the vector field  $V^\mu$  will be hided for simplicity in some cases.

and

$$V_{H,\phi} = \lambda_m \phi^\dagger \phi H^\dagger H, \quad (2.3)$$

$$V_{H,S} = \frac{\delta_2}{2} H^\dagger H |\mathbb{S}|^2, \quad (2.4)$$

$$V_{\phi,S} = \frac{\delta_1}{2} \phi^\dagger \phi |\mathbb{S}|^2, \quad (2.5)$$

where  $D^\mu \phi = \partial^\mu \phi - i \frac{g_\phi}{2} \tau \cdot V'^\mu$ . The hidden gauge coupling  $g_\phi < 4\pi$ , required by the unitarity bound, need to be hold for any thermal particle whose relic density arises from the freeze-out of its annihilation [39, 45, 46]. In particular,  $b_1$  and  $a_1$  terms break the global  $U(1)$  symmetry explicitly. In the SM Lagrangian, the Higgs potential notations are defined as:  $\mathcal{L}^{SM} \ni -(m^2/2)H^\dagger H - \lambda(H^\dagger H)^2$  with  $H = (0, v + h)/\sqrt{2}$ , where  $v$  is the VEV of the Higgs field.

After the  $SU(2)_D$  being spontaneously broken, both  $\phi$  and the singlet  $\mathbb{S}$  get the VEVs:

$$\phi = (0, \frac{v_\phi + \eta'}{\sqrt{2}}), \quad (2.6)$$

$$\mathbb{S} = \frac{1}{\sqrt{2}}(v_s + S + iA). \quad (2.7)$$

So the Eq. (2.1) in the unitary gauge recast as,

$$\begin{aligned} \mathcal{L} = & \mathcal{L}_{SM} - \frac{1}{4} F_{\mu\nu} \cdot F^{\mu\nu} + \frac{1}{8} (g_\phi v_\phi)^2 V_\mu \cdot V^\mu \\ & + \frac{1}{8} g_\phi^2 V_\mu \cdot V^\mu \eta'^2 + \frac{1}{4} g_\phi^2 v_\phi V_\mu \cdot V^\mu \eta' + \frac{1}{2} (\partial_\mu \eta')^2 \\ & + V_{h,\eta',S,A}, \end{aligned} \quad (2.8)$$

here  $V^\mu = UV'^\mu U^{-1} - \frac{i}{g} [\partial_\mu U] U^{-1}$  with  $U = \exp(-i\tau \cdot \xi/v_\phi)$ . The vector DM mass is given by  $m_V = g_\phi v_\phi/2$ , and the tree-level potential  $V_0(h, \eta', S, A)$  recast as,

$$\begin{aligned} V_0(h, \eta', S, A) = & \frac{m^2}{4} (h + v)^2 + \frac{\mu_\phi^2}{4} (\eta' + v_\phi)^2 - \frac{\lambda_\phi}{16} (\eta' + v_\phi)^4 + \frac{1}{4} \lambda (h + v)^4 \\ & + \frac{1}{4} \lambda_m (h + v)^2 (\eta' + v_\phi)^2 + \frac{1}{8} (\delta_2 (h + v)^2 + \delta_1 (\eta' + v_\phi)^2) ((S + v_s)^2 + A^2) \\ & + \frac{1}{4} (b_2 - b_1) (S + v_s)^2 + \frac{1}{4} (b_2 + b_1) A^2 - \sqrt{2} a_1 (S + v_s) + \frac{d_2}{8} (S + v_s)^2 A^2 \\ & + \frac{d_2}{16} ((S + v_s)^4 + A^4). \end{aligned} \quad (2.9)$$

Here, we would like to mention that,  $\eta'$  lives in the fundamental representation of  $SU(2)_D$ , and displays a custodial symmetry  $SO(3)$  in the  $V_{1,2,3}^\mu$  component space, which makes three  $V_i^\mu$  components degenerate in mass and thus stable [47]. The explicit  $Z_2$ -breaking term is proportional to  $a_1$  and being introduced here to avoid the cosmological domain wall problem [48–50]. After choosing  $\phi_{a_1} = \phi_{b_1} = \pi$ , the potential retains a  $Z_2$  symmetry for  $\text{Im}(\mathbb{S})$ , thereby ensuring the stability of the particle  $A$  [51, 52].

Requiring that the potential in Eq. (2.9) has a minimum at  $\langle H \rangle = h/\sqrt{2} = 0$  and  $\langle S \rangle = S + iA = 0 + i \cdot 0$ , the following minimization conditions are obtained:

$$\frac{\partial V_0}{\partial h} = 0, \quad \frac{\partial V_0}{\partial \eta} = 0, \quad \frac{\partial V_0}{\partial S} = 0, \quad \frac{\partial V_0}{\partial A} = 0, \quad (2.10)$$

where all derivatives are evaluated at  $(h, \eta, S, A) = (0, 0, 0, 0)$ . These minimization conditions allow the Higgs VEV  $v$  and the singlet VEV  $v_s$  to replace  $m^2$  and  $b_2$  according to

$$\begin{aligned} m^2 &\equiv -\frac{1}{2}(4v^2\lambda + v_s^2\delta_2 - 2v_\phi^2\lambda_m), \\ \mu_\phi^2 &\equiv -\frac{1}{2}(\delta_1 v_s + 2\lambda_m v^2 + \lambda_\phi v_\phi^2), \\ b_2 &\equiv \frac{1}{2v_s}(4\sqrt{2}a_1 - v_s(-2b_1 + d_2 v_s^2 + \delta_1 v_\phi^2 + \delta_2 v^2)). \end{aligned} \quad (2.11)$$

Thus, at the minima, the mass matrix is obtained as

$$M = \begin{pmatrix} 2\lambda v^2 & \lambda_m v v_\phi & \frac{1}{2}\delta_2 v_s v & 0 \\ \lambda_m v v_\phi & \frac{1}{2}\lambda_\phi v_\phi^2 & \frac{1}{2}\delta_1 v_s v_\phi & 0 \\ \frac{1}{2}\delta_2 v_s v & \frac{1}{2}\delta_1 v_s v_\phi & \frac{2\sqrt{2}a_1 + v_s^3 d_2}{v_s} & 0 \\ 0 & 0 & 0 & \frac{a_1}{2\sqrt{2}v_s} + b_1 \end{pmatrix}. \quad (2.12)$$

And in the basis of  $(h, \eta', S)$ , we have

$$M = \begin{pmatrix} 2\lambda v^2 & \lambda_m v v_\phi & \frac{1}{2}\delta_2 v_s v \\ \lambda_m v v_\phi & \frac{1}{2}\lambda_\phi v_\phi^2 & \frac{1}{2}\delta_1 v_s v_\phi \\ \frac{1}{2}\delta_2 v_s v & \frac{1}{2}\delta_1 v_s v_\phi & \frac{2\sqrt{2}a_1 + v_s^3 d_2}{v_s} \end{pmatrix}. \quad (2.13)$$

To work in the mass eigenstates, i.e.,  $h_{1,2,3}$ , we diagonalise the mass matrix Eq. (2.13) through

$$RM^2R^T = M_{diag}^2, \quad (2.14)$$

with matrix  $R$  being given by

$$R = \begin{pmatrix} c_1 c_3 & c_3 s_1 & s_3 \\ c_2 s_1 - c_1 s_2 s_3 & c_1 c_2 - s_1 s_2 s_3 & c_3 s_2 \\ s_1 s_2 - c_1 c_2 s_3 & c_1 s_2 - c_2 s_1 s_3 & c_2 c_3 \end{pmatrix}, \quad (2.15)$$

$c, s$  and their subscripts 1, 2, 3 represent  $\cos, \sin, \theta_{12}, \theta_{23}$ , and  $\theta_{13}$  individually.

### 3 Dark matter analysis

In our model, we have two component DMs. Thus, to present the novelty of the model properly, we use the coupled boltzman equations explored in [3], with annihilation channels being depicted in Fig. 1, and details of annihilation cross sections are listed in section A. The relic density of each component DM could be obtained through  $\Omega_{A,V} h^2 = 2.755 \times 10^8 \frac{M_{A,V}}{\text{GeV}} Y_{A,V}(T_0)$  [53, 54] after we calculated  $Y_{A,V}(T_0)$  numerically, and the total relic

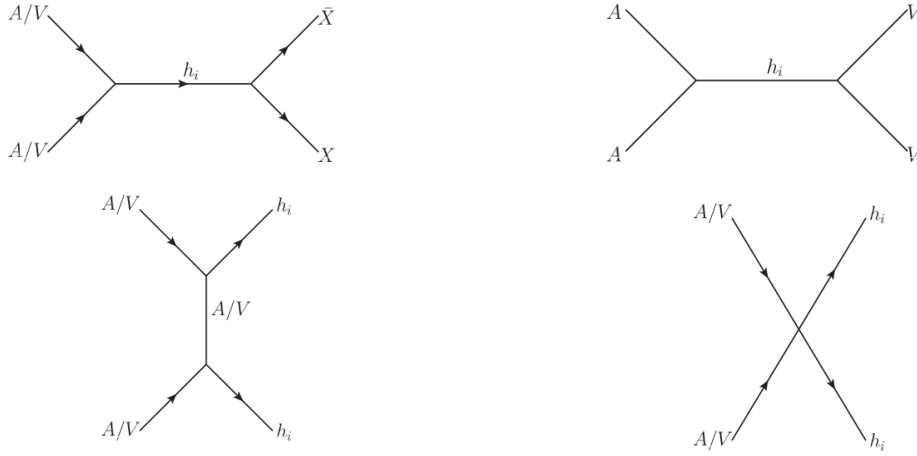


**Figure 1.** Feynman diagrams of annihilation channels.

density is the sum of the two component DMs,  $\Omega h^2 = \Omega_A h^2 + \Omega_V h^2$ . As for the numerical calculations of  $Y_{A,V}(T_0)$ , we refer to Eqs. (B.1), (B.2), (B.3), and (B.4).

In order to investigate how does the interplay between the two DM components affect the evolution of the DM abundance and the dependence of the DM relic density on each parameters, we scan the parameter spaces according to the following three groups:

1. Scan in the  $M_A - M_V$  plane for the case of  $M_A > M_V$ , with the other parameters being given in Table 1.
2. Scan in the  $M_A - M_V$  plane for the case of  $M_A < M_V$ , with the other parameters being given in Table 1.
3. Scan in the  $\lambda_m - \delta_2$  plane, with DM masses being fixed as:  $M_V=120$  GeV,  $M_A=150$  GeV, and the other parameters are given in Table 2.

$v$	$v_\phi$	$v_s$	$\lambda$	$\lambda_\phi$	$d_2$	$\delta_1$	$\delta_2$	$\lambda_m$	$g_\phi$
246	738	123	0.515	0.2	0.2	0.02	0.04	0.01	0.04

**Table 1.** The input parameters for the analyses of the cases of  $m_A > m_V$  and  $m_A < m_V$ .

$v$	$v_\phi$	$v_s$	$\lambda$	$\lambda_\phi$	$d_2$	$\delta_1$
246	738	123	0.515	0.2	0.21	0.02

**Table 2.** The VEVs of three scalar fields and other couplings.

### 3.1 Relic density analysis

Set free parameters as in Table 1, the three Higgs masses are obtained as  $m_{h_1} = 124.8$ ,  $m_{h_2} = 233.8$ , and  $m_{h_3} = 71.1$  GeV in order.

### 1. The first group with $m_A > m_V$

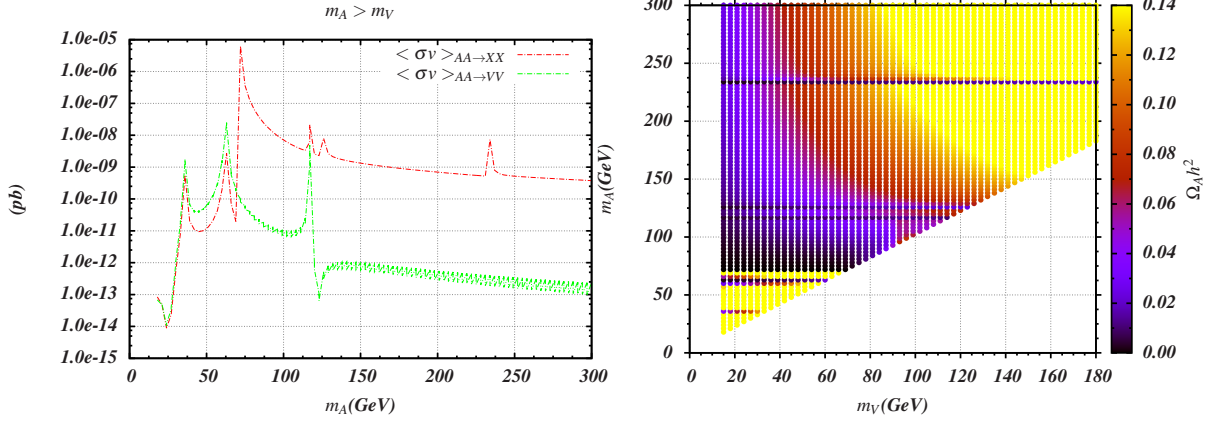


**Figure 2.** Left: Plots for the cross sections of channels  $AA \rightarrow XX$  and  $AA \rightarrow VV$  in units of  $0.3894 \times 10^9 \text{ pb}$ ; Right: The corresponding relic density  $\Omega_A h^2$ .

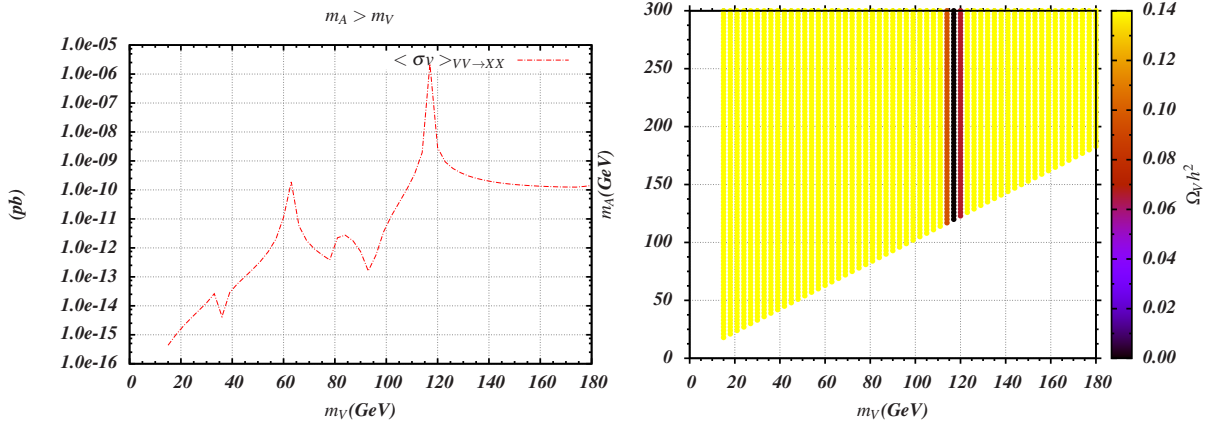


**Figure 3.** Left: Plot of the cross sections of channel  $VV \rightarrow XX$  in units of  $0.3894 \times 10^9 \text{ pb}$ ; Right: Corresponding relic density  $\Omega_V h^2$  for  $m_A > m_V$ .

The annihilation channel  $AA \rightarrow VV$  is opened up and shown by the green line on the left panel of Fig. 2. The bandwidth of the green line comes from the change of the vector DM mass  $m_V$ , and the bandwidth becomes wider and wider with the increasing of scalar DM mass  $m_A$ , since the bigger the scalar DM mass  $m_A$  the larger viable range will be left for  $m_V$ . Fig. 2 depicts that the channel  $AA \rightarrow XX$  is the dominate one when  $m_A > 70 \text{ GeV}$ , and the variation tendency of the relic density  $\Omega_A h^2$  is plotted in the right panel. Three peaks of the annihilation cross section of  $AA \rightarrow VV$  are presented, at  $m_A = m_{h_1}/2, m_{h_2}/2, m_{h_3}/2$ , those are the three resonances at these mass values, as could be seen from Eq. (A.6) as well. At the same time, we find three other peaks of the annihilation cross section of  $AA \rightarrow XX$ , besides the same three peaks as that of  $AA \rightarrow VV$ , at  $m_A = m_{h_i}$  (the three masses of three Higgs),



because the new partial  $t$ ,  $u$  and seagull channels  $AA \rightarrow h_i h_i$  through exchanging the scalar DM particle themselves are opened up around these mass values. These peaks represent themselves on the right panel of Fig. 2 by the transition of the color along axis of  $m_A$ . When there is a peak bigger than about  $1 \times 10^{-9}$  for the cross section (on the left panel), a decrease behavior of the corresponding relic density appears on the right panel.

Last but not the least, we would like to emphaze that the opening of the channel  $AA \rightarrow VV$  does cause the decrease of the magnitude of  $\Omega_A h^2$ . Because of  $\Omega_A h^2 \sim 1/\langle\sigma v\rangle_{AA \rightarrow XX}$ , when the channel  $AA \rightarrow VV$  has been shut down, one may expect  $\langle\sigma v\rangle_{AA \rightarrow XX} \sim pb$  and  $\Omega_A h^2 \sim 0.1$ . While, the right panel of Fig. 2 depicts more decrease of the magnitude of  $\Omega_A h^2$  around  $m_A = m_{h_{1,2}}/2$ , which demonstrates the effects of the annihilation process  $AA \rightarrow VV$ .

For the case of  $m_A > m_V$ , as shown in Fig. 3, the channel of  $VV \rightarrow AA$  is closed when we analyzing  $\Omega_V h^2$ . The cross section of the channel  $AA \rightarrow VV$  together with that of  $VV \rightarrow XX$  affect the corresponding relic density  $\Omega_V h^2$ , and the second one dominates the value of  $\Omega_V h^2$ . Only the slim peak caused by the resonance at about  $m_V = m_{h_2}/2$  brings a sizable decreasing of  $\Omega_V h^2$ . The viable region of  $m_V$  matching the experimental value  $\Omega h^2 = 0.1189$  [55] ( $\Omega_V h^2$ ) is very small as shown in the right panel.

## 2. The second group with $m_V > m_A$

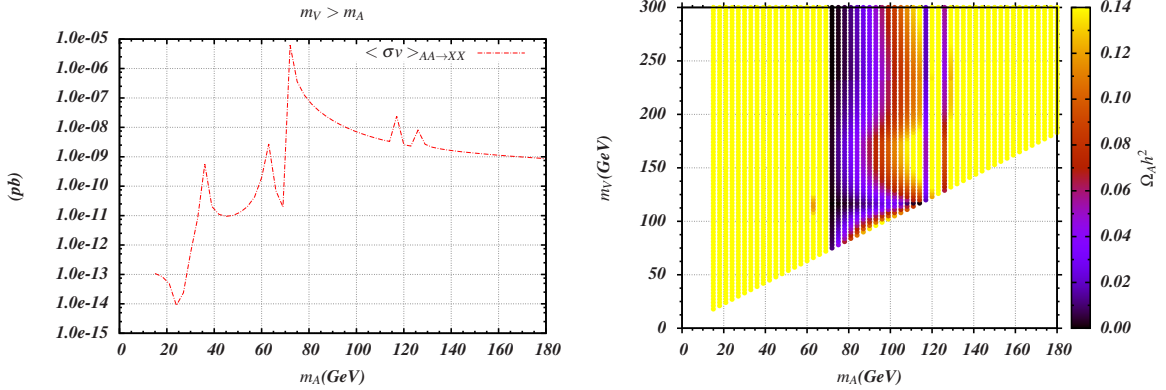


**Figure 4.**  $m_V > m_A$ . Left: Plots for annihilation cross section of channel  $AA \rightarrow XX$  in units of  $0.3894 \times 10^9 pb$ ; Right: Relic density  $\Omega_A h^2$ .

In this case, the channel  $AA \rightarrow VV$  is forbidden due to  $m_V > m_A$ , and the behavior of the cross section of the channel  $AA \rightarrow XX$  is given in the left panel of Fig. 4. With the increasing of  $m_A$ , the first peak caused by the resonance effect does not leave any trails, as could be seen in the magnitude of the corresponding relic density (see the right panel of Fig. 4), because the magnitude of the cross section is too small. The second peak is caused by the resonance effect at  $m_A = m_{h_1}/2$ , and the tinny increasing of cross section induces a small decreasing of the corresponding relic

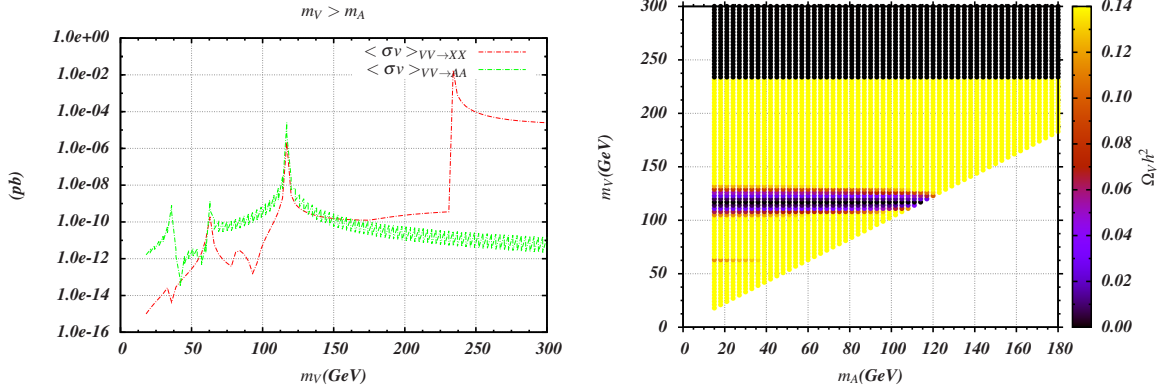


**Figure 5.**  $m_V > m_A$ . Left: Plots for the cross sections of annihilation channels  $VV \rightarrow XX$  and  $VV \rightarrow AA$  in units of  $0.3894 \times 10^9$  pb; Right: The dominating relic density  $\Omega_V h^2$ .

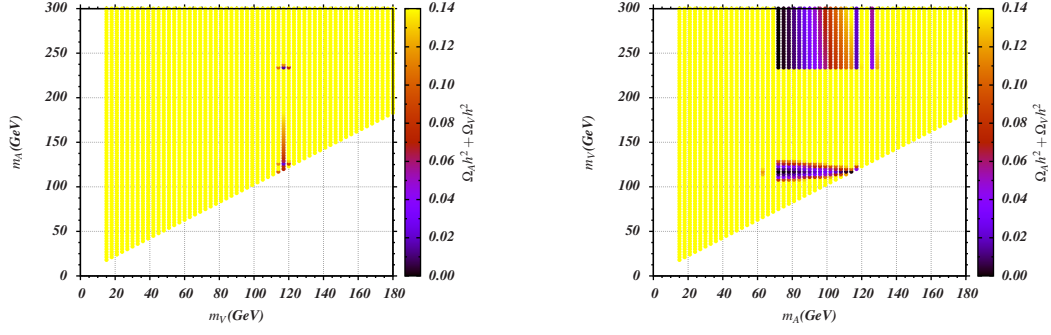
density. The third peak demonstrates the opening up of the partial  $t$  and  $u$  channels for  $AA \rightarrow h_3 h_3$  and also brings a very big decrease of the relic density at about  $m_A \geq m_{h_3}$  as expected. And the fourth peak, which is caused by the resonance at  $m_A = m_{h_2}/2$ , brings a sizable decrease of the magnitude of the relic density also. We also notice the small waves at about  $m_V = 160$  GeV in the right panel of Fig. 4. The phenomenon could be explained by Eq. (B.4), which illustrates that the behavior of the cross section  $\langle \sigma v \rangle_{VV \rightarrow AA}$  affects the calculation of  $\Omega_A h^2$  and the variation of the magnitude of the cross section  $\langle \sigma v \rangle_{VV \rightarrow AA}$  generates these small waves. The channel  $VV \rightarrow AA$  also causes a bigger decrease of the magnitude of  $\Omega_V h^2$  in comparison with the scenario in which the channel  $VV \rightarrow AA$  has been shut down, as shown in the right panel of Fig. 5, especially around  $m_V \sim m_{h_1}/2 (m_{h_1})$ .

Fig. 5 is plotted to show the magnitude of  $\Omega_V h^2$  contributing from both channels  $VV \rightarrow XX$  and  $VV \rightarrow AA$ . The cross sections are small for most regions, and a big decrease of  $\Omega_V h^2$  exists in the two regions  $m_V \sim m_{h_2}/2$  and  $m_V > m_{h_2}$ . For the first decrease, both channels induce comparable effects. And for the second decrease, it is the channel  $VV \rightarrow XX$  that dominates the magnitude of  $\Omega_V h^2$ . Especially when  $m_V > m_{h_2}$ , the partial  $t$ ,  $u$  and seagull channels  $VV \rightarrow h_2 h_2$  through exchanging the vector DM particle are opened up. These effects give rise to too big  $\langle \sigma v \rangle_{VV \rightarrow XX}$ , and then the door to generate relic density  $\Omega_V h^2$  is almost closed.

At last, the two panels in the Fig. 6 presents the total relic density for  $m_A > m_V$  and  $m_V > m_A$ , respectively. Under the set of parameters as in the Table 1, the large enough magnitude of the relic density could be obtained easily.

### 3. The third group: varying $\lambda_m$ and $\delta_2$

FIG. 7 depicts the relationships among  $\delta_2$ ,  $\lambda_m$  and the cross sections. FIG. 8 illustrates that the magnitude of  $\Omega_A h^2 (\Omega_V h^2)$  reaches its critical value around  $\delta_2 \sim 0.09$  ( $\lambda_m \sim 0.01$ ). And that the DM relic density for each component almost depends on their



**Figure 6.** Plots of the total relic density  $\Omega_A h^2 + \Omega_V h^2$  for the case of  $m_A > m_V$  and  $m_V > m_A$ .

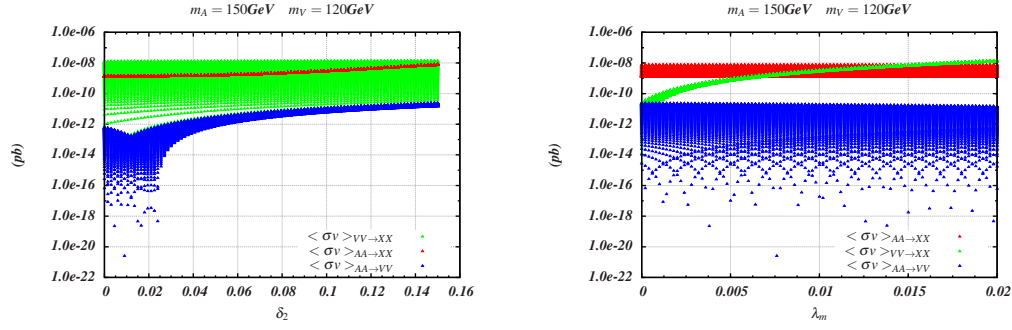


**Figure 7.** Plots of  $\delta_2$  and  $\lambda_m$  vs. cross sections.

own coupling parameters, this is caused by the fact that all related annihilation cross sections are proportional to  $\delta_2$  or  $\lambda_m$ .

### 3.2 Direct detection

In our model, the two component DMs, i.e., the scalar  $A$  and vector  $V$ , interact with the SM particles through the exchange of three Higgs bosons. Thus, the DM-nucleon scattering cross section is spin-independent (SI). For each single component, the SI DM-nucleon cross sections are calculated to be

$$\sigma_{SI}^A = \frac{1}{16\pi v^2} \frac{m_N^4 f_N^2}{(m_A + m_N)^2} \left| \frac{\delta_2 v}{2} \frac{R_{11}}{m_{h_1}^2} + \frac{\delta_1 v_\phi}{2} \frac{R_{21}}{m_{h_2}^2} + \frac{d_2 v_s}{2} \frac{R_{31}}{m_{h_3}^2} \right|^2, \quad (3.1)$$

$$\sigma_{SI}^V = \frac{1}{16\pi v^2} \frac{m_N^4 f_N^2}{(m_V + m_N)^2} \left| g_\phi^2 v_\phi \frac{R_{21} R_{11}}{m_{h_1}^2} + g_\phi^2 v_\phi \frac{R_{22} R_{21}}{m_{h_2}^2} + g_\phi^2 v_\phi \frac{R_{23} R_{31}}{m_{h_3}^2} \right|^2, \quad (3.2)$$

with  $R_{ij}$  coming from Eq. (2.15),  $m_N$  and  $f_N = \sum f_L + 3 \times \frac{2}{27} f_H$  are the nucleon mass and effective Higgs-nucleon coupling respectively, where  $f_N$  is the summation of light quark ( $f_L$ ) and heavy quark ( $f_H$ ) contributions, and we take the value  $f_N = 0.326$  [56] in our numerical analysis. Since the current experiments assume that the local DM density is provided by one single DM specie, the situation that both  $A$ ,  $V$  components contribute

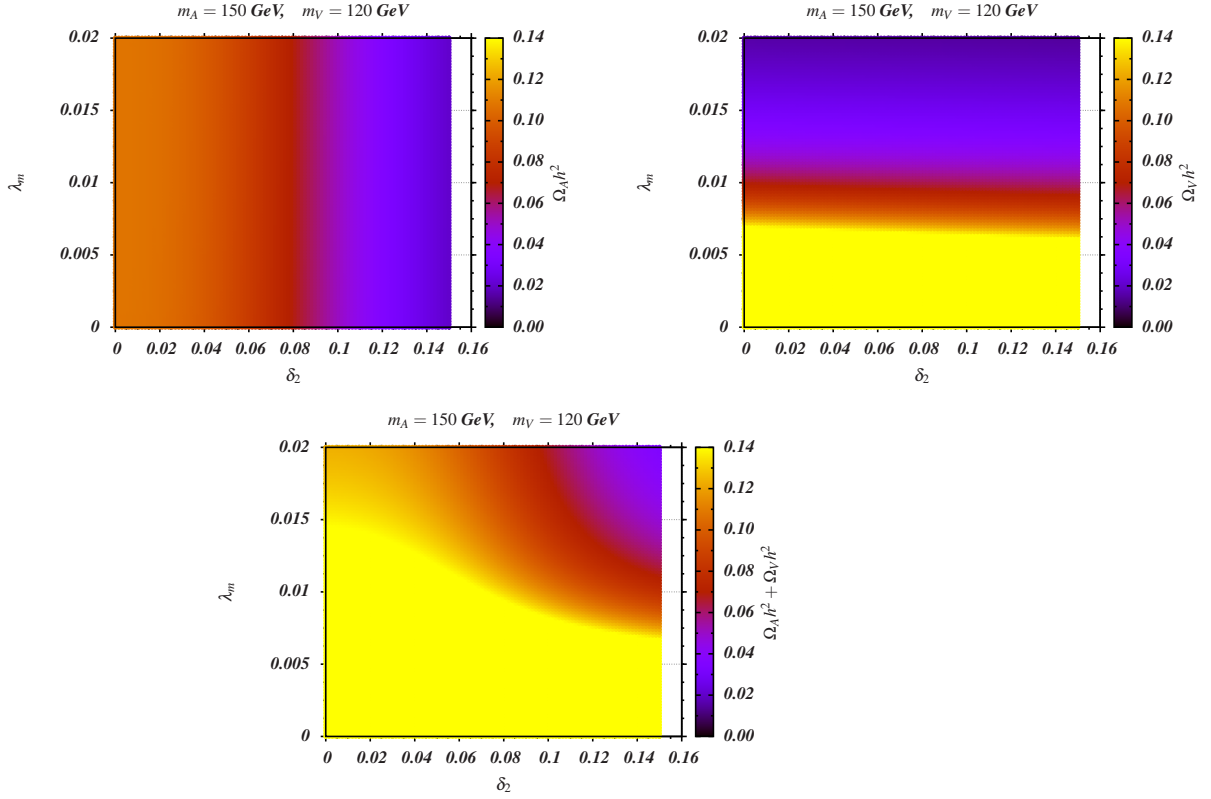


**Figure 8.** Plots of  $\delta_2$  and  $\lambda_m$  *vs.* relic density.

to the local DM density making us unable to use the current experimental results directly. Assuming the contribution of each DM component to the local density is the same as their contribution to the relic density, the SI scattering cross section should be rescaled by a factor  $\Omega_{A,V}h^2/\Omega_{DM}h^2$ . Thus, the corresponding upper limit on the SI DM-nucleon cross section of each single component is [38, 52]:

$$\sigma_{SI}^A \leq (\Omega_{DM}h^2/\Omega_S h^2)\sigma_{SI}^{exp}(M_A), \quad (3.3)$$

$$\sigma_{SI}^V \leq (\Omega_{DM}h^2/\Omega_V h^2)\sigma_{SI}^{exp}(M_V). \quad (3.4)$$

Similar to the above Section, here we do analyses using the LUX experiment results [57] via three groups as well.

1.  $m_A > m_V$

The left and right panels of Fig. 9 depict that: with the value of  $m_V$  being unbounded,  $m_A$  should be bigger than 30 GeV.

2.  $m_V > m_A$

The left and right panels of Fig. 10 depict that  $m_{A,V}$  should be no smaller than 50 GeV.

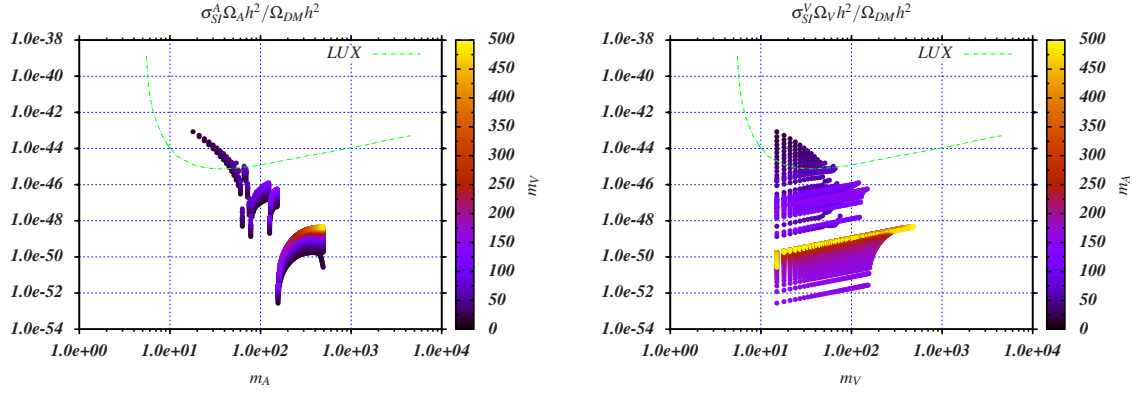


**Figure 9.** For the case of  $m_A > m_V$ , parameter regions being left considering the direct detection constraint of LUX.

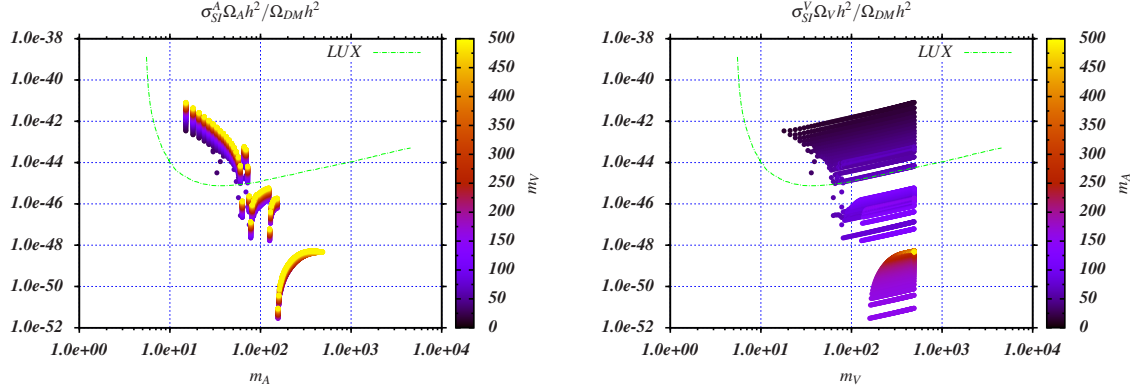


**Figure 10.** For the case of  $m_V > m_A$ , parameter regions being left considering the direct detection constraint of LUX.

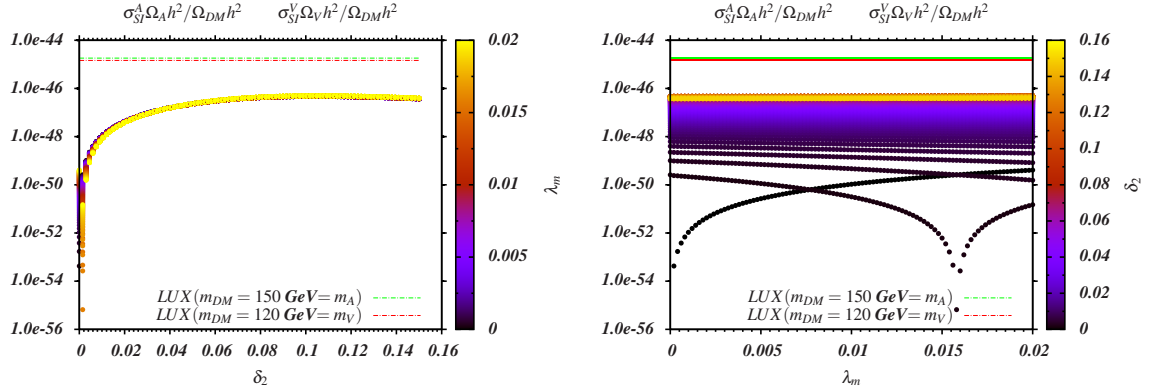


**Figure 11.**  $\delta_2$  and  $\lambda_m$ . Parameter regions being left considering the direct detection constraints on the model coefficients.

### 3. parameter space of $\delta_2$ and $\lambda_m$

Fig. 11 depicts that all the parameter spaces satisfy the experimental constraints.

## 4 Higgs indirect search and electroweak precision constraints

In this section, we study the effects of the mixing among the three fields  $h$ ,  $\eta'$ ,  $S$  using the Higgs indirect search and constraints from electroweak precision observables.

### 4.1 Higgs indirect search

The current status of the LHC measurements of the Higgs couplings constrains the matrix element  $R_{11}$ , which describes the discrepancy between  $h_1$  and the SM Higgs. The couplings of  $h_1$  to all SM particles are the rescaled values of the SM couplings, taking the form of

$$g_{h_1 XX} = R_{11} g_{h_1 XX}^{SM} . \quad (4.1)$$

For the first two group parameter spaces in the last Section, additional decay channel  $h_1 \rightarrow AA(VV)$  exists, which almost does not change the total width, since we have the square of  $R_{12}(R_{13})$  to suppress the magnitude of  $\Gamma(h_1 \rightarrow AA(VV))$ . The same logic applies to the analysis with the third parameter group used in the last Section <sup>4</sup>. Thus signal rates  $\mu_{XX}$  associated with Higgs measurements are functions of  $R_{11}$

$$\mu_{XX} = \frac{\sigma \cdot BR}{\sigma^{SM} \cdot BR^{SM}} = R_{11}^2 , \quad (4.2)$$

with  $\sigma$ ,  $BR$  (that with a superscript  $SM$ ) being the production cross section and branching ratios of  $h_1$  (the SM Higgs). Therefore, to what extent the model differs from the SM Higgs measurements is determined by the value of  $R_{11}$ . The value of  $R_{11}$  for the parameter setup given in Table. 1 is 0.9973, and we refer to Fig. 12 for the  $R$  values<sup>5</sup> corresponding to the benchmark scenario given in Table. 2.

### 4.2 Electroweak precision observables constraints

The presence of the scalar  $h_3$  with mass  $m_{h_3} < 114$  GeV is subject to tight bounds from the LEP [58], while these bounds are highly released in all our parameter choices, since the mixing between  $h_1$  and  $h_3$  is very small, about 0.0573 for benchmark scenario given in Table. 1 and could be seen in the Fig. 12 for the benchmark scenario given in Table. 2.

As for electroweak precision observables, the oblique parameters  $S$  and  $T$  which parameterize potential new physics contributions to electroweak radiative corrections, are

---

<sup>4</sup>Because the mass of  $h_2(h_3)$  is above the threshold, additional channel  $h_1 \rightarrow h_2 h_2(h_3 h_3)$ , which changes the total width, does not open. For the study of one Higgs decays to two other Higgs bosons, we refer to [59].

<sup>5</sup>Here, we use  $R(i, j)$  as the labels in the two plots, which means the same as that of  $R_{ij}$  in other place of this work.

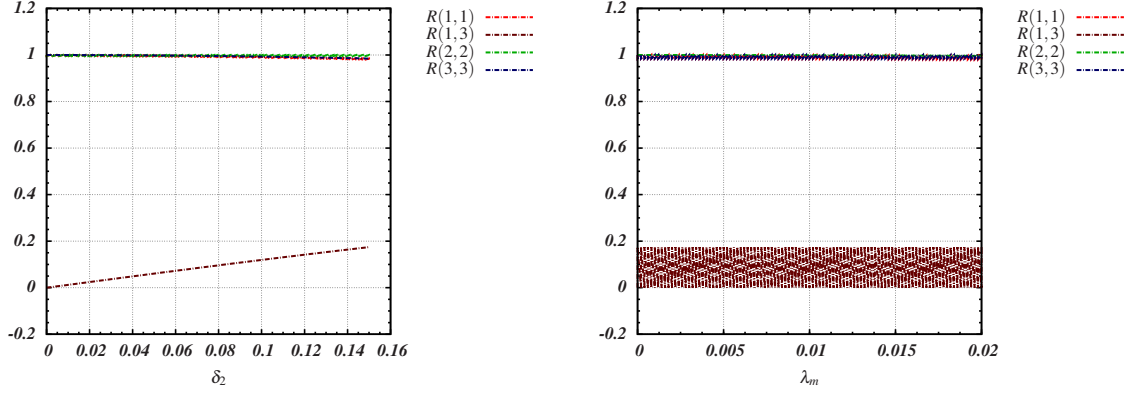


**Figure 12.**  $R$  values with respect to  $\lambda_m$  and  $\delta_2$ .

computed following Refs. [47, 60]. In our model, they are

$$S = \frac{1}{24\pi} \left\{ R_{11}^2 [\log R_{h_1 h} + G(m_{h_1}^2, m_Z^2) - G(m_{h_1}^2, m_Z^2)] \right. \\ \left. + R_{12}^2 [\log R_{h_2 h} + G(m_{h_2}^2, m_Z^2) - G(m_{h_2}^2, m_Z^2)] \right. \\ \left. + R_{13}^2 [\log R_{h_3 h} + G(m_{h_3}^2, m_Z^2) - G(m_{h_3}^2, m_Z^2)] \right\}, \quad (4.3)$$

$$T = \frac{3}{16\pi \sin^2 \theta_W} \left\{ R_{11}^2 \left[ \frac{1}{\cos^2 \theta_W} \left( \frac{\log R_{Zh_1}}{1 - R_{Zh_1}} - \frac{\log R_{Zh}}{1 - R_{Zh}} \right) - \left( \frac{\log R_{Wh_1}}{1 - R_{Wh_1}} - \frac{\log R_{Wh}}{1 - R_{Wh}} \right) \right] \right. \\ \left. + R_{12}^2 \left[ \frac{1}{\cos^2 \theta_W} \left( \frac{\log R_{Zh_2}}{1 - R_{Zh_2}} - \frac{\log R_{Zh}}{1 - R_{Zh}} \right) - \left( \frac{\log R_{Wh_2}}{1 - R_{Wh_2}} - \frac{\log R_{Wh}}{1 - R_{Wh}} \right) \right] \right. \\ \left. + R_{13}^2 \left[ \frac{1}{\cos^2 \theta_W} \left( \frac{\log R_{Zh_3}}{1 - R_{Zh_3}} - \frac{\log R_{Zh}}{1 - R_{Zh}} \right) - \left( \frac{\log R_{Wh_3}}{1 - R_{Wh_3}} - \frac{\log R_{Wh}}{1 - R_{Wh}} \right) \right] \right\}, \quad (4.4)$$

where,  $R_{AB}$ ,  $G(m_A^2, m_B^2)$  and  $f(R_{AB})$  are given by

$$R_{AB} = \frac{m_A^2}{m_B^2}, \quad (4.5)$$

$$G(m_A^2, m_B^2) = -\frac{79}{3} + 9R_{AB} - 2R_{AB}^2 + (12 - 4R_{AB} + R_{AB}^2)f(R_{AB}) \\ + (-10 + 18R_{AB} - 6R_{AB}^2 + R_{AB}^3 - 9\frac{R_{AB} + 1}{R_{AB} - 1})\log R_{AB}, \quad (4.6)$$

$$f(R_{AB}) = \begin{cases} \sqrt{R_{AB}(R_{AB} - 4)} \log \left| \frac{R_{AB} - 2 - \sqrt{R_{AB}(R_{AB} - 4)}}{2} \right| & R_{AB} > 4, \\ 0 & R_{AB} = 4, \\ 2\sqrt{R_{AB}(4 - R_{AB})} \arctan \sqrt{\frac{4 - R_{AB}}{R_{AB}}} & R_{AB} < 4. \end{cases} \quad (4.7)$$

The parameters set is given in Table 2 and the magnitude of  $g_\phi$  is determined by  $m_V$  and  $v_\phi$ . The constraints on two parameters  $\delta_2$  and  $\lambda_m$  from  $S$  and  $T$  parameters are shown

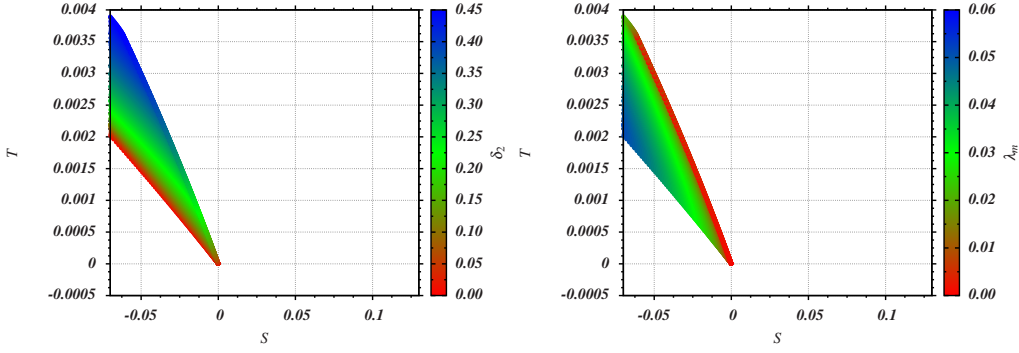


**Figure 13.** Constraints on  $\delta_2$ ,  $\lambda_m$  from limits of  $S$  and  $T$ .

in Fig. 13. The  $S$  and  $T$  constraints require that  $\delta_2$  and  $\lambda_m$  should be smaller than about 0.45 and 0.06 respectively.  $S$  and  $T$  are very sensitive to the mixing effects. The first two parameter groups (as given in Section 3.1) does not change the mixing angles among  $h, \eta', S$ , and  $S$  and  $T$  give rise to the null limits since the mixing effects among  $h$  and  $\eta'$ ,  $S$  in that cases are very small.

## 5 Vacuum stability

The global minimum of the tree-level potential of our model requires,

$$\lambda > 0, \lambda_\phi > 0, d_2 > 0, \lambda d_2 > 4\delta_2^2, \lambda_\phi d_2 > \delta_1^2, \lambda\lambda_\phi > 16\lambda_m^2. \quad (5.1)$$

From one-loop renormalization group equations (RGEs) of the Higgs quartic couplings in Appendix C, i.e., Eq. (C.1), we find that the Higgs portals couplings  $\lambda_m$  and  $\delta_2$  are all get involved and give rise to positive contributions to  $\beta_\lambda$ . Thus, we could expect the vacuum stability problem being solved or alleviated in some parameter spaces. Adopting the central values of top quark mass, the Higgs mass, and the strong coupling [55] as the low energy boundary conditions, we find that with the increasing energy scale, the Higgs quartic coupling running to a negative value around the scale  $10^9$  GeV, and then grows to positive values latter [61, 62].

Based on arguments on vacuum stability given in Ref. [62], one needs have positive value of the Higgs quartic coupling to ensure absolute stability. It is obvious that to obtain absolute stability, we should elevate the curves of the Higgs quartic coupling in the plot of  $\lambda - \mu$  [61, 62]. From the  $\beta$  functions given in Eq. (C.1), we find that with the increasing of  $\lambda_m$  and  $\delta_2$  one could have the increasing of the value of the Higgs quartic coupling  $\lambda$ . To verify this, we explore parameter spaces that survive under  $S$  and  $T$  limits as shown in Fig. 14, and we find that  $\lambda_m$  and  $\delta_2$  are required to be bigger than around 0.35 in order to evade the stability problem.

To figure out to what extent we need to lift the value of the Higgs quartic coupling in the third parameters setup (as given in Table 2), we plot contours of  $\lambda(\mu = 10^9 \text{ (} 10^{18} \text{)})$



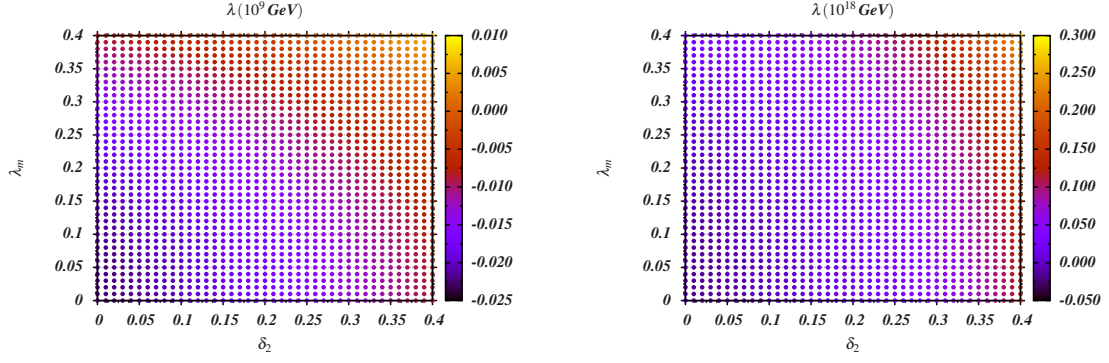


**Figure 14.** The Higgs quartic coupling  $\lambda$  as a function of  $\lambda_m$  and  $\delta_2$  at  $10^9$  GeV (left panel) and  $10^{18}$  GeV (right panel). With parameters set as:  $\lambda = 0.129$ ,  $\lambda_\phi = 0.2$ ,  $d_2 = 0.2$ ,  $\delta_1 = 0.2$ ,  $\delta_2 = 0.2$ ,  $\lambda_m = 0.2$ .

GeV) with respect to  $\lambda_m$  and  $\delta_2$ , as shown in Fig. 15, and we find that the vacuum is not bound from below there. The plot of  $\lambda$  (at the scale of  $10^9$  GeV) as a function of  $\lambda_m$  and  $\delta_2$ , for the scenario with two  $\mathbb{S}$  being supplemented (both two  $\mathbb{S}$  have the same interaction with the SM and the  $SU(2)_D$  group), shows that with  $\delta_2 > 0.25$  one can indeed obtain the potential bounded from below, as shown in Fig. 16. The two figures, i.e., Fig. 15 and Fig. 16, illustrate that to achieve the vacuum stability, no smaller than two  $\mathbb{S}$  is expected in the third parameters setup.

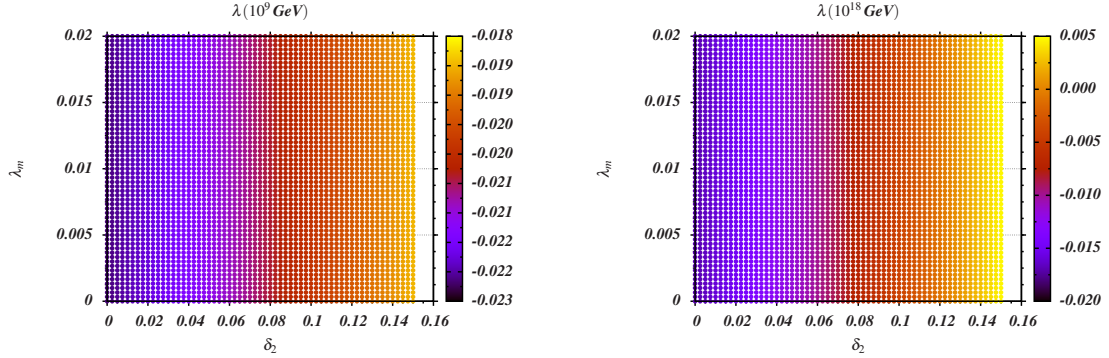


**Figure 15.** The Higgs quartic coupling  $\lambda$  as a function of  $\lambda_m$  and  $\delta_2$  at  $10^9$  GeV (left panel) and  $10^{18}$  GeV (right panel). With parameters set as:  $\lambda = 0.515$ ,  $\lambda_\phi = 0.2$ ,  $d_2 = 0.2$ ,  $\delta_1 = 0.02$ ,  $\delta_2 = 0.04$ ,  $\lambda_m = 0.01$ .

## 6 Footprint of the naturalness problem

In this section, we would like to present the relevant naturalness problem in our model, and discuss the indirect search of the scenario which could improve the naturalness problem.

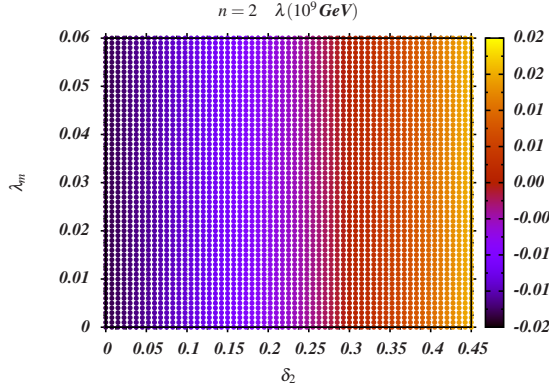


**Figure 16.**  $\lambda(10^9 \text{ GeV})$  as a function of  $\delta_2$  and  $\lambda_m$ .  $n = 2$  is to indicate we have supplemented two  $\mathbb{S}$ .

### 6.1 The naturalness problem

In the SM, considering the gauge invariant property of the two point Higgs Green function [63], the naturalness problem could be defined as

$$(m_h^0)^2 = m_h^2 + \frac{\Lambda^2}{(4\pi)^2} VC_{SM} , \quad (6.1)$$

where

$$VC_{SM} = 12\lambda - 12g_t^2 + \frac{9}{2}g_2^2 + \frac{3}{2}g_1^2 , \quad (6.2)$$

and  $m_h$  ( $m_h^0$ ) is the renormalized (bare) Higgs mass,  $\Lambda$  indicates the cut off scale where the new fields are required to cancel the quadratic divergences of the Higgs mass square.

Although our model is renormalizable, we assume it as a low energy effective theory of some more fundamental theory, which is UV completed at the scale  $\Lambda$ . Thus, Eq. (6.2) becomes

$$(m_h^0)^2 = m_h^2 + \frac{\Lambda^2}{(4\pi)^2} VC_{VA} , \quad (6.3)$$

with

$$\begin{aligned} VC_{VA} \approx & 12\lambda + \frac{9}{2}g_2^2 + \frac{3}{2}g_1^2 - 12g_t^2 \\ & + \frac{5}{2}\lambda_m + \frac{\lambda_m^2}{\lambda_\phi} + \frac{3g_\phi^2\lambda_m}{2\lambda_\phi} + n\left(\frac{3}{8}\delta_2 + \frac{\delta_2\lambda_m}{\lambda_\phi}\right. \\ & \left. + \frac{\delta_2^2 d_2}{8} + \frac{\delta_2\delta_1}{8d_2}\right) , \end{aligned} \quad (6.4)$$

in which new fields get involved. Here, we suppose that not only one  $\mathbb{S}$  embracing the same property as explored in the model (thus  $n$  is introduced to denote the number of  $\mathbb{S}$ ), and

the symbol  $\approx$  is to indicate that Eq. (6.3) could be hold in the case where  $S$ ,  $\eta'$ , and  $H$  have negligible mixing.

In addition, we would like to mention that, the VEV and Higgs mass in the SM are gauge invariant considering the renormalization of the mass term in the SM Higgs potential [64]. And [64] use the different tadpole renormalization method in comparison with that of [63] and leaves no trails of tadpole contributions in  $VC_{SM}$  and  $VC_{VA}$ , which cast the new formula of

$$\begin{aligned} VC'_{SM} &= -(6\lambda - 6g_t + \frac{9}{4}g_2^2 + \frac{3}{4}g_1^2) , \\ VC'_{VA} &\approx -(6\lambda + \frac{9}{4}g_2^2 + \frac{3}{4}g_1^2 - 6g_t^2) - \frac{1}{2}\lambda_m - \frac{n}{2}\delta_2 . \end{aligned} \quad (6.5)$$

To soften the naturalness problem [4, 5], the simplest solution is to suppose  $VC_{VA} = 0$  (or  $VC'_{VA} = 0$ ) so that the modified Veltman condition [65] is realized. For  $\Lambda = 10$  TeV,  $n \approx 1(6)$  is needed to obtain  $VC_{VA} = 0$  ( $VC'_{VA} = 0$ ).

## 6.2 Indirect search for the scenario which alleviates the naturalness problem

Considering  $m_{\eta', S, A} \gg v$  could been satisfied in some parameter spaces of the model <sup>6</sup>, one may integrate out the  $\eta', S, A$  and express their effects in terms of an effective Lagrangian below the scale  $Min(m_{\eta'}, m_S, m_A)$ , which involves only the SM fields with appropriate higher-dimensional operators. At one-loop level, integrating out the  $\eta', S, A$  leads to shifts in the wave-function renormalization and the potential of the Higgs doublet  $H$ , as well as operators with dimension six and higher. The dimension-six operators in the effective Lagrangian cast the form of

$$\mathcal{L}_{eff} = \mathcal{L}_{SM} + (\frac{c_H^{\eta'}}{m_{\eta'}^2} + \frac{c_H^S}{m_S^2} + \frac{c_H^A}{m_A^2}) \left( \frac{1}{2} \partial_\mu |H|^2 \partial^\mu |H|^2 \right) . \quad (6.6)$$

Matching to the full theory at the scale  $m_{\eta', s, A}$ , we have

$$\begin{aligned} c_H^{\eta'} &= \frac{n_{\eta'}}{4} |\lambda_m|^2 / (96\pi^2) , \\ c_H^S &= \frac{n}{8} |\delta_2|^2 / (96\pi^2) , \\ c_H^A &= \frac{n}{8} |\delta_2|^2 / (96\pi^2) . \end{aligned} \quad (6.7)$$

Below the scale of electroweak symmetry breaking, Eq. (6.6) leads to a shift in the wave-function renormalization of the physical scalar  $h$  [9], with  $\delta Z_h = 2v^2(c_H^{\eta'}/m_{\eta'}^2 + c_H^S/m_S^2 + c_H^A/m_A^2)$ . After canonically normalizing  $h$ , i.e.,  $h \rightarrow (1 - \delta Z_h/2)h$ , its coupling to vectors and fermions are altered, which may lead to a measurable correction to, e.g., the  $hZ$  associated production cross-section

$$\delta\sigma_{Zh} = -2v^2(c_H^{\eta'}/m_{\eta'}^2 + c_H^S/m_S^2 + c_H^A/m_A^2) , \quad (6.8)$$

---

<sup>6</sup>For simplicity, we consider the case in which the mixings among the three fields  $\eta', S, A$  could be neglected.

where we have defined  $\delta\sigma_{Zh}$  as the fractional change in the associated production cross section relative to the SM prediction, which by design vanishes for the case of the SM.<sup>7</sup> The sizable  $n_{\eta'}(n)$ , being required to relax the naturalness problem<sup>8</sup> (see Eq. (6.3)), may causes the correspondingly observable effect in the precision measurement of  $\sigma_{Zh}$ , which is what the future lepton colliders supposed to detect. At last, if one use our model to analyze electroweak phase transition, the measurement of associated production cross section of  $Zh$  ( $\sigma_{Zh}$ ) might imposes very strong constraint on the multi-Higgs portals couplings  $\lambda_m$  and  $\delta_2$ .

## 7 Discussions and conclusion

In our model, the vector field ( $V$ ) and the imaginary part of complex singlet ( $A$ ) are stable due to the reduced custodial symmetry  $SO(3)$  and the residual  $Z_2$  symmetry. The interactions between the two DMs and resonant effects mediated by three Higgs portals are demonstrated through the study of the relic density behavior with respect to  $m_A$  and  $m_V$ . The effects of the multi-Higgs portals couplings on the generation of DM relic density are shown in the parameter space of  $\lambda_m$  and  $\delta_2$ . The parameter spaces of  $\lambda_m$  and  $\delta_2$  are totally free under the LUX experiment results limits. Constraints (from LUX experimental results) on parameter spaces of  $m_A - m_V$  give rise to  $m_A > 30$  GeV ( $m_A(m_V) > 50$  GeV) for the case of  $m_A > m_V$  ( $m_A < m_V$ ), which allows more relaxed parameter spaces in compare with the simple models. As for the third parameter group: the electroweak precision observables require  $\lambda_m < 0.06$  and  $\delta_2 < 0.45$ , the vacuum stability at high scale requires at least two complex singlet, which is supposed to be consistent with the naturalness problem argument. Other benchmark scenario with one  $\mathbb{S}$ , which survives under indirect Higgs search and electroweak precision test limits, and could improve the stability problem is also explored.

At last, we would like to mention that, through tuning of the parameter  $\delta_2$  associate with tuning of  $v_s$  in the first setup of parameter spaces<sup>9</sup>, one could use the model to explain Galactic Center Excess observed by the Fermi Telescope, with  $\langle\sigma v\rangle \approx 10^{-26}$   $\text{cm}^3/\text{s}$  being provided by scalar DM pairs annihilating to  $b\bar{b}$  and the relic density supplied by the vector DM<sup>10</sup>. Details of which, and the realization of SFOEWPT and inflation in the model are left for further studies.

---

<sup>7</sup>Here, we would like to mention that, which one of  $c_H^\eta$ ,  $c_H^s$ ,  $c_H^A$  in the our model takes part in  $\delta\sigma_{Zh}$  depends on parameter choices, i.e, the derivations of  $c_H^{\eta'}$ ,  $c_H^s$ ,  $c_H^A$  require  $m_{\eta',S,A} \gg v$ .

<sup>8</sup> The sizable  $n$  is also necessary from the viewpoint of the vacuum stability, see Section 5.

<sup>9</sup>In order to maintain small mixing between  $h$  and  $S$  which helps to escape constraints of LHC and electroweak observable experiments.

<sup>10</sup>For a viable annihilating multi-component dark matter model consisting of two real gauge singlet scalars, one can explain the low energy (1 – 3 GeV) gamma ray excess from both Galactic Centre and Fermi Bubble [67].

## A Annihilation Cross Sections

When the Higgs mass  $m_{h_i}$  is larger than twice of the SM particle masses, the corresponding visible decay channels widths are

$$\Gamma_{h_i \rightarrow ff} = \frac{N_c G_F m_f^2}{4\sqrt{2}\pi} m_{h_i} |R_{i1}|^2 \left(1 - \frac{4m_f^2}{m_{h_i}^2}\right)^{3/2}, \quad (\text{A.1})$$

$$\Gamma_{h_i \rightarrow WW} = \frac{G_F}{8\sqrt{2}\pi} m_{h_i}^3 |R_{i1}|^2 \sqrt{1 - \frac{4m_W^2}{m_{h_i}^2}} \left(1 - \frac{4m_W^2}{m_{h_i}^2} + \frac{12m_W^4}{m_{h_i}^4}\right), \quad (\text{A.2})$$

$$\Gamma_{h_i \rightarrow ZZ} = \frac{G_F}{16\sqrt{2}\pi} m_{h_i}^3 |R_{i1}|^2 \sqrt{1 - \frac{4m_Z^2}{m_{h_i}^2}} \left(1 - \frac{4m_Z^2}{m_{h_i}^2} + \frac{12m_Z^4}{m_{h_i}^4}\right), \quad (\text{A.3})$$

and when the Higgs mass  $m_{h_i}$  is larger than the twice of the DM mass, the invisible decay channels widths are

$$\Gamma_{h_i \rightarrow VV} = \left| R_{i2} g_\phi^2 \frac{v_\phi}{v} \right|^2 \frac{v^2 m_{h_i}^3}{128\pi m_V^4} \sqrt{1 - \frac{4m_V^2}{m_{h_i}^2}} \left(1 - \frac{4m_V^2}{m_{h_i}^2} + \frac{12m_V^4}{m_{h_i}^4}\right), \quad (\text{A.4})$$

$$\Gamma_{h_i \rightarrow AA} = \left| R_{i1} \frac{\delta_2}{2} + R_{i2} \frac{\delta_1}{2} \frac{v_\phi}{v} + R_{i3} \frac{d_2}{2} \frac{v_s}{v} \right|^2 \frac{v^2}{32\pi m_{h_i}} \sqrt{1 - \frac{4m_A^2}{m_{h_i}^2}}. \quad (\text{A.5})$$

The total decay widths of the Higgs with mass  $m_{h_i}$  are the summations of visible and invisible decay widths.

The annihilation cross sections for DM corresponding to Fig. 1 are given as follows:

- **Top-left**

$$\begin{aligned} \langle \sigma v \rangle_{VV \rightarrow h_j h_j}^s &= \frac{1}{32\pi} \frac{g_\phi^4 v_\phi^2}{m_V^2} \sqrt{1 - \frac{m_{h_1}^2}{m_V^2}} \\ &\times \left| \left[ \sum_i \frac{R_{2i} \left( R_{i1} R_{1j} \lambda v + R_{i2} R_{2j} \lambda_m v_\phi + R_{i3} R_{3j} \frac{\delta_2}{2} v_s \right)}{4m_V^2 - m_{h_i}^2 + i m_{h_i} \Gamma_{h_i}} \right] \right|^2, \\ \langle \sigma v \rangle_{VV \rightarrow ff} &= n_c \sum_f \frac{m_f^2}{16\pi} \left(1 - \frac{m_f^2}{m_V^2}\right)^{3/2} \left| \sum_i \frac{(g_\phi^2 v_\phi / v) R_{2i} R_{i1}}{4m_V^2 - m_{h_i}^2 + i m_{h_i} \Gamma_{h_i}} \right|^2, \end{aligned}$$

$$\begin{aligned}
\langle \sigma v \rangle_{VV \rightarrow ZZ} &= \frac{m_V^2}{128\pi} \sqrt{1 - \frac{m_Z^2}{m_V^2}} \left( 1 - \frac{m_Z^2}{m_V^2} + \frac{3m_Z^4}{m_V^4} \right) \left| \sum_i \frac{(g_\phi^2 v_\phi / v) R_{2i} R_{i1}}{4m_V^2 - m_{h_i}^2 + im_{h_i} \Gamma_{h_i}} \right|^2, \\
\langle \sigma v \rangle_{VV \rightarrow WW} &= \frac{m_V^2}{64\pi} \sqrt{1 - \frac{m_W^2}{m_V^2}} \left( 1 - \frac{m_W^2}{m_V^2} + \frac{3m_W^4}{m_V^4} \right) \left| \sum_i \frac{(g_\phi^2 v_\phi / v) R_{2i} R_{i1}}{4m_V^2 - m_{h_i}^2 + im_{h_i} \Gamma_{h_i}} \right|^2, \\
\langle \sigma v \rangle_{AA \rightarrow h_j h_j}^s &= \frac{1}{32\pi} \frac{1}{m_A^2} \sqrt{1 - \frac{m_{h_1}^2}{m_A^2}} \\
&\quad \times \left| \frac{\delta_2}{2} v \left[ \sum_i \frac{R_{1i} \left( R_{i1} R_{1j} \lambda v + R_{i2} R_{2j} \lambda_m v_\phi + R_{i3} R_{3j} \frac{\delta_2}{2} v_s \right)}{4m_A^2 - m_{h_i}^2 + im_{h_i} \Gamma_{h_i}} \right] \right. \\
&\quad + \frac{\delta_1}{2} v_\phi \left[ \sum_i \frac{R_{2i} \left( R_{i1} R_{1j} \lambda v + R_{i2} R_{2j} \lambda_m v_\phi + R_{i3} R_{3j} \frac{\delta_2}{2} v_s \right)}{4m_A^2 - m_{h_i}^2 + im_{h_i} \Gamma_{h_i}} \right] \\
&\quad \left. + \frac{d_2}{2} v_s \left[ \sum_i \frac{R_{3i} \left( R_{i1} R_{1j} \lambda v + R_{i2} R_{2j} \lambda_m v_\phi + R_{i3} R_{3j} \frac{\delta_2}{2} v_s \right)}{4m_A^2 - m_{h_i}^2 + im_{h_i} \Gamma_{h_i}} \right] \right|^2, \\
\langle \sigma v \rangle_{AA \rightarrow ff} &= n_c \sum_f \frac{m_f^2}{16\pi} \left( 1 - \frac{m_f^2}{m_A^2} \right)^{3/2} \left| \left[ \sum_i \frac{(\delta_2/2) R_{1i} R_{i1}}{4m_A^2 - m_{h_i}^2 + im_{h_i} \Gamma_{h_i}} \right] \right. \\
&\quad \times \left[ \sum_i \frac{(\delta_1 v_\phi / 2v) R_{2i} R_{i1}}{4m_A^2 - m_{h_i}^2 + im_{h_i} \Gamma_{h_i}} \right] + \left[ \sum_i \frac{(d_2 v_s / 2v) R_{3i} R_{i1}}{4m_A^2 - m_{h_i}^2 + im_{h_i} \Gamma_{h_i}} \right] \left. \right|^2, \\
\langle \sigma v \rangle_{AA \rightarrow ZZ} &= \frac{m_A^2}{128\pi} \sqrt{1 - \frac{m_Z^2}{m_A^2}} \left( 1 - \frac{m_Z^2}{m_A^2} + \frac{3m_Z^4}{m_A^4} \right) \times \left| \left[ \sum_i \frac{(\delta_2/2) R_{1i} R_{i1}}{4m_A^2 - m_{h_i}^2 + im_{h_i} \Gamma_{h_i}} \right] \right. \\
&\quad + \left[ \sum_i \frac{(\delta_1 v_\phi / 2v) R_{2i} R_{i1}}{4m_A^2 - m_{h_i}^2 + im_{h_i} \Gamma_{h_i}} \right] + \left[ \sum_i \frac{(d_2 v_s / 2v) R_{3i} R_{i1}}{4m_A^2 - m_{h_i}^2 + im_{h_i} \Gamma_{h_i}} \right] \left. \right|^2, \\
\langle \sigma v \rangle_{AA \rightarrow WW} &= \frac{m_A^2}{64\pi} \sqrt{1 - \frac{m_W^2}{m_A^2}} \left( 1 - \frac{m_W^2}{m_A^2} + \frac{3m_W^4}{m_A^4} \right) \times \left| \left[ \sum_i \frac{(\delta_2/2) R_{1i} R_{i1}}{4m_A^2 - m_{h_i}^2 + im_{h_i} \Gamma_{h_i}} \right] \right. \\
&\quad + \left[ \sum_i \frac{(\delta_1 v_\phi / 2v) R_{2i} R_{i1}}{4m_A^2 - m_{h_i}^2 + im_{h_i} \Gamma_{h_i}} \right] + \left[ \sum_i \frac{(d_2 v_s / 2v) R_{3i} R_{i1}}{4m_A^2 - m_{h_i}^2 + im_{h_i} \Gamma_{h_i}} \right] \left. \right|^2.
\end{aligned}$$

• **Top-right**

$$\begin{aligned}
\langle \sigma v \rangle_{VV \rightarrow AA} &= \frac{1}{32\pi} \frac{1}{m_V^2} \sqrt{1 - \frac{m_A^2}{m_V^2}} \left| \left[ \sum_i \frac{(g_\phi^2 v_\phi) R_{2i} \left( R_{i1} \frac{\delta_2}{2} v + R_{i2} \frac{\delta_1}{2} v_\phi + R_{i3} \frac{d_2}{2} v_s \right)}{4m_V^2 - m_{h_i}^2 + im_{h_i} \Gamma_{h_i}} \right] \right|^2, \\
\langle \sigma v \rangle_{AA \rightarrow VV} &= \frac{m_A^2}{128\pi} \sqrt{1 - \frac{m_V^2}{m_A^2}} \left( 1 - \frac{m_V^2}{m_A^2} + \frac{3m_V^4}{m_A^4} \right) \times \left| \left[ \sum_i \frac{(\delta_2/2) R_{1i} R_{i1}}{4m_A^2 - m_{h_i}^2 + im_{h_i} \Gamma_{h_i}} \right] \right|^2.
\end{aligned}$$

$$+ \left[ \sum_i \frac{(\delta_1 v_\phi/2v) R_{2i} R_{i1}}{4m_A^2 - m_{h_i}^2 + im_{h_i} \Gamma_{h_i}} \right] + \left[ \sum_i \frac{(d_2 v_s/2v) R_{3i} R_{i1}}{4m_A^2 - m_{h_i}^2 + im_{h_i} \Gamma_{h_i}} \right] \Big|^2.$$

• **Bottom-left**

$$\begin{aligned} \langle \sigma v \rangle_{VV \rightarrow h_i h_i}^{t+u} &= \frac{1}{4\pi} \frac{1}{m_V^2} \sqrt{1 - \frac{m_{h_i}^2}{m_V^2}} \left| \frac{(g_\phi^2 v_\phi)^2}{m_{h_i}^2 - m_V^2} \right|^2 R_{2i}^2, \\ \langle \sigma v \rangle_{AA \rightarrow h_i h_i}^{t+u} &= \frac{1}{4\pi} \frac{1}{m_A^2} \left[ \sqrt{1 - \frac{m_{h_1}^2}{m_A^2}} \left| \frac{(\delta_2 v/2)^2 R_{1i}}{m_{h_1}^2 - m_A^2} \right|^2 + \sqrt{1 - \frac{m_{h_2}^2}{m_A^2}} \left| \frac{(\delta_1 v_\phi/2)^2 R_{2i}}{m_{h_2}^2 - m_A^2} \right|^2 \right. \\ &\quad \left. + \sqrt{1 - \frac{m_{h_3}^2}{m_A^2}} \left| \frac{(d_2 v_s/2)^2 R_{3i}}{m_{h_3}^2 - m_A^2} \right|^2 \right]. \end{aligned}$$

• **Bottom-right**

$$\begin{aligned} \langle \sigma v \rangle_{VV \rightarrow h_i h_i}^{seagull} &= \frac{1}{32\pi} \frac{1}{m_V^2} \sqrt{1 - \frac{m_{h_i}^2}{m_V^2}} \left| \frac{g_\phi^2}{2} \right|^2 R_{2i}^2, \\ \langle \sigma v \rangle_{AA \rightarrow h_i h_i}^{seagull} &= \frac{1}{32\pi} \frac{1}{m_A^2} \left[ \sqrt{1 - \frac{m_{h_1}^2}{m_A^2}} \left| \frac{\delta_2}{2} \right|^2 R_{1i}^2 + \sqrt{1 - \frac{m_{h_2}^2}{m_A^2}} \left| \frac{\delta_1 v_\phi}{2 v} \right|^2 R_{2i}^2 \right. \\ &\quad \left. + \sqrt{1 - \frac{m_{h_3}^2}{m_A^2}} \left| \frac{d_2 v_s}{2 v} \right|^2 R_{3i}^2 \right]. \end{aligned}$$

## B Boltzman equations

The coupled boltzman equations could be written as [3]:

$$\begin{aligned} \frac{dY_A}{dx_A} &= -\frac{1.32g_\star^{1/2} M_A M_p}{x_A^2} \left( \langle \sigma v_{rel} \rangle_{AA \rightarrow X \bar{X}} (Y_A^2 - (Y_A^{eq})^2) \right. \\ &\quad \left. + \langle \sigma v_{rel} \rangle_{AA \rightarrow VV} \left( Y_A^2 - \frac{(Y_A^{eq})^2}{(Y_V^{eq})^2} Y_V^2 \right) \right), \end{aligned} \quad (B.1)$$

$$\begin{aligned} \frac{dY_V}{dx_V} &= -\frac{1.32g_\star^{1/2} M_V M_p}{x_V^2} \left( \langle \sigma v_{rel} \rangle_{VV \rightarrow X \bar{X}} (Y_V^2 - (Y_V^{eq})^2) \right. \\ &\quad \left. - \langle \sigma v_{rel} \rangle_{AA \rightarrow VV} \left( Y_A^2 - \frac{(Y_A^{eq})^2}{(Y_V^{eq})^2} Y_V^2 \right) \right), \end{aligned} \quad (B.2)$$

for  $M_A > M_V$ .

Similarly, for  $M_V > M_A$ , one has

$$\begin{aligned} \frac{dY_V}{dx_V} = & -\frac{1.32g_\star^{1/2}M_V M_p}{x_V^2} \left( \langle \sigma v_{rel} \rangle_{VV \rightarrow X\bar{X}} (Y_V^2 - (Y_V^{eq})^2) \right. \\ & \left. + \langle \sigma v_{rel} \rangle_{VV \rightarrow AA} \left( Y_V^2 - \frac{(Y_V^{eq})^2}{(Y_A^{eq})^2} Y_A^2 \right) \right), \end{aligned} \quad (\text{B.3})$$

$$\begin{aligned} \frac{dY_A}{dx_A} = & -\frac{1.32g_\star^{1/2}M_A M_p}{x_A^2} \left( \langle \sigma v_{rel} \rangle_{AA \rightarrow X\bar{X}} (Y_A^2 - (Y_A^{eq})^2) \right. \\ & \left. - \langle \sigma v_{rel} \rangle_{VV \rightarrow AA} \left( Y_V^2 - \frac{(Y_V^{eq})^2}{(Y_A^{eq})^2} Y_A^2 \right) \right). \end{aligned} \quad (\text{B.4})$$

Here,  $M_p = 2.44 \times 10^{18}$  GeV is the reduced Planck mass, and  $g_\star$  is the degrees of freedom parameter. Two dimensionless variables  $Y_{i,j}$  relate with number density through  $Y_{i,j} = \frac{n_{i,j}}{s}$ ,  $x_{i,j} = \frac{m_{i,j}}{T}$  [66], and  $s$  and  $T$  are the entropy density and temperature of the Universe. After solving the coupled Eqs. (B.1), (B.2), (B.3), and (B.4), one gets the values of  $Y_A$  and  $Y_V$  at present temperature  $T_0$ .

## C One loop $\beta$ functions

The one-loop renormalization group equations (RGEs), which we used to analyze the vacuum stability problem, are given by

$$\frac{dX}{d \log \mu} = \frac{1}{16\pi^2} \beta_X, \quad (\text{C.1})$$

with one-loop  $\beta$ -functions  $\beta_X$ ,

$$\beta_{\delta_1} = \frac{1}{2} (4d_2\delta_1 - 9g_\phi^2\delta_1^2 + 4\delta_1^2 + 3\delta_1\lambda_\phi + 2\lambda_m\delta_2), \quad (\text{C.2})$$

$$\beta_{\delta_2} = \frac{1}{2} (4d_2\delta_2 - 3g_1^2\delta_2 - 9g_2^2\delta_2 + 12g_t^2\delta_2 + 4\delta_2^2 + 12\delta_2\lambda + 2\delta_1\lambda_m), \quad (\text{C.3})$$

$$\beta_{d_2} = \frac{1}{2} (10d_2^2 + \delta_1^2 + \delta_2^2), \quad (\text{C.4})$$

$$\beta_{\lambda_m} = \frac{1}{2} (\delta_1\delta_2 - 3g_1^2\lambda_m - 9g_2^2\lambda_m + 12g_t^2\lambda_m - 9g_\phi^2\lambda_m + 12\lambda\lambda_m + 8\lambda_m^2 + 3\lambda_m\lambda_\phi), \quad (\text{C.5})$$

$$\beta_\lambda = -\lambda(3g_1^2 + 9g_2^2 - 12g_t^2 - 24\lambda) + \frac{3}{4}g_2^4 + \frac{3}{8}(g_1^2 + g_2^2)^2 - 6g_t^4 + \frac{\delta_2^2}{4} + \frac{\lambda_m^2}{2}, \quad (\text{C.6})$$

$$\beta_{\lambda_\phi} = \frac{1}{2} (9g_\phi^4 + 2\delta_1^2 + 4\lambda_m^2 - 18g_\phi^2\lambda_\phi + 9\lambda_\phi^2), \quad (\text{C.7})$$

$$\beta_{g_\phi} = -\frac{43}{6}g_\phi^3. \quad (\text{C.8})$$

## Acknowledgments

LGB thank Michael Ramsey-Musolf, Ran Ding and Bin Zhu for useful discussions. This research was supported in part by the Natural Science Foundation of China under grant numbers 10821504, 11075194, 11135003, 11275246, and 11475238, and by the National Basic Research Program of China (973 Program) under grant number 2010CB833000.



## References

- [1] G. Aad *et al.* [ATLAS Collaboration], Phys. Lett. B **716**, 1 (2012) [arXiv:1207.7214 [hep-ex]].
- [2] S. Chatrchyan *et al.* [CMS Collaboration], Phys. Lett. B **716**, 30 (2012) [arXiv:1207.7235 [hep-ex]].
- [3] L. Bian, R. Ding and B. Zhu, Phys. Lett. B **728**, 105 (2014) [arXiv:1308.3851 [hep-ph]].
- [4] I. Chakraborty and A. Kundu, Phys. Rev. D **87**, no. 5, 055015 (2013) [arXiv:1212.0394 [hep-ph]].
- [5] B. Grzadkowski and J. Wudka, Phys. Rev. Lett. **103**, 091802 (2009) [arXiv:0902.0628 [hep-ph]].
- [6] C. N. Karahan and B. Korutlu, Phys. Lett. B **732**, 320 (2014) [arXiv:1404.0175 [hep-ph]].
- [7] O. Antipin, M. Mojaza and F. Sannino, Phys. Rev. D **89**, 085015 (2014) [arXiv:1310.0957 [hep-ph]].
- [8] B. Henning, X. Lu and H. Murayama, arXiv:1404.1058 [hep-ph].
- [9] N. Craig, C. Englert and M. McCullough, Phys. Rev. Lett. **111**, no. 12, 121803 (2013) [arXiv:1305.5251 [hep-ph]].
- [10] C. Englert and M. McCullough, JHEP **1307**, 168 (2013) [arXiv:1303.1526 [hep-ph]].
- [11] M. Farina, M. Perelstein and N. R. L. Lorier, Phys. Rev. D **90**, 015014 (2014) [arXiv:1305.6068 [hep-ph]].
- [12] A. Noble and M. Perelstein, Phys. Rev. D **78**, 063518 (2008) [arXiv:0711.3018 [hep-ph]].
- [13] P. H. Damgaard, D. O’Connell, T. C. Petersen and A. Tranberg, Phys. Rev. Lett. **111**, no. 22, 221804 (2013) [arXiv:1305.4362 [hep-ph]].
- [14] S. Profumo, M. J. Ramsey-Musolf, C. L. Wainwright and P. Winslow, arXiv:1407.5342 [hep-ph].
- [15] H. Davoudiasl, I. Lewis and E. Ponton, Phys. Rev. D **87**, no. 9, 093001 (2013) [arXiv:1211.3449 [hep-ph]].
- [16] M. S. Carena, A. Megevand, M. Quiros and C. E. M. Wagner, Nucl. Phys. B **716**, 319 (2005) [hep-ph/0410352].
- [17] M. Gonderinger, Y. Li, H. Patel and M. J. Ramsey-Musolf, JHEP **1001**, 053 (2010) [arXiv:0910.3167 [hep-ph]].
- [18] A. Drozd, B. Grzadkowski and J. Wudka, JHEP **1204**, 006 (2012) [arXiv:1112.2582 [hep-ph]].
- [19] S. Baek, P. Ko, W. I. Park and E. Senaha, JHEP **1305**, 036 (2013) [arXiv:1212.2131 [hep-ph]].
- [20] S. Baek, P. Ko and W. I. Park, JHEP **1307**, 013 (2013) [arXiv:1303.4280 [hep-ph]].
- [21] E. Gabrielli, M. Heikinheimo, K. Kannike, A. Racioppi, M. Raidal and C. Spethmann, Phys. Rev. D **89**, 015017 (2014) [arXiv:1309.6632 [hep-ph]].
- [22] T. Hambye and A. Strumia, Phys. Rev. D **88**, 055022 (2013) [arXiv:1306.2329 [hep-ph]].
- [23] P. Ko and W. I. Park, arXiv:1405.1635 [hep-ph].
- [24] N. Haba and R. Takahashi, Phys. Rev. D **89**, 115009 (2014) [arXiv:1404.4737 [hep-ph]].
- [25] Gintaras Duda, Graciela Gelmini, and Paolo Gondolo. Detection of a subdominant density component of cold dark matter. *Phys.Lett.*, B529:187–192, 2002, hep-ph/0102200.
- [26] Gintaras Duda, Graciela Gelmini, Paolo Gondolo, Joakim Edsjo, and Joseph Silk. Indirect detection of a subdominant density component of cold dark matter. *Phys.Rev.*, D67:023505, 2003, hep-ph/0209266.
- [27] Stefano Profumo, Kris Sigurdson, and Lorenzo Ubaldi. Can we discover multi-component WIMP dark matter? *JCAP*, 0912:016, 2009, 0907.4374.

- [28] X. Gao, Z. Kang and T. Li, *Eur. Phys. J. C* **69**, 467 (2010) [arXiv:1001.3278 [hep-ph]].
- [29] Daniel Feldman, Zuowei Liu, Pran Nath, and Gregory Peim. Multicomponent Dark Matter in Supersymmetric Hidden Sector Extensions. *Phys.Rev.*, D81:095017, 2010, 1004.0649.
- [30] Howard Baer, Andre Lessa, Shibi Rajagopalan, and Warintorn Sreethawong. Mixed axion/neutralino cold dark matter in supersymmetric models. *JCAP*, 1106:031, 2011, 1103.5413.
- [31] Mayumi Aoki, Michael Duerr, Jisuke Kubo, and Hiroshi Takano. Multi-Component Dark Matter Systems and Their Observation Prospects. *Phys.Rev.*, D86:076015, 2012, 1207.3318.
- [32] D. Chialva, P. S. B. Dev and A. Mazumdar, *Phys. Rev. D* **87**, no. 6, 063522 (2013) [arXiv:1211.0250 [hep-ph]].
- [33] Subhadittya Bhattacharya, Aleksandra Drozd, Bohdan Grzadkowski, and Jose Wudka. Two-Component Dark Matter. *JHEP*, 1310:158, 2013, 1309.2986.
- [34] Yuji Kajiyama, Hiroshi Okada, and Takashi Toma. Multicomponent dark matter particles in a two-loop neutrino model. *Phys.Rev.*, D88(1):015029, 2013, 1303.7356.
- [35] S. Esch, M. Klasen and C. E. Yaguna, *JHEP* **1409**, 108 (2014) [arXiv:1406.0617 [hep-ph]].
- [36] K. R. Dienes and B. Thomas, *Phys. Rev. D* **85**, 083523 (2012) [arXiv:1106.4546 [hep-ph]]; *Phys. Rev. D* **85**, 083524 (2012) [arXiv:1107.0721 [hep-ph]].
- [37] K. R. Dienes, S. Su and B. Thomas, *Phys. Rev. D* **86**, 054008 (2012) [arXiv:1204.4183 [hep-ph]]; K. R. Dienes, J. Kumar and B. Thomas, *Phys. Rev. D* **86**, 055016 (2012) [arXiv:1208.0336 [hep-ph]]; K. R. Dienes, J. Kumar and B. Thomas, *Phys. Rev. D* **88**, no. 10, 103509 (2013) [arXiv:1306.2959 [hep-ph]]; K. R. Dienes, S. Su and B. Thomas, arXiv:1407.2606 [hep-ph].
- [38] G. Belanger and J. C. Park, *JCAP* **1203**, 038 (2012) [arXiv:1112.4491 [hep-ph]].
- [39] O. Lebedev, H. M. Lee and Y. Mambrini, *Phys. Lett. B* **707**, 570 (2012) [arXiv:1111.4482 [hep-ph]].
- [40] K. Griest and M. Kamionkowski, *Phys. Rev. Lett.* **64**, 615 (1990).
- [41] H. Davoudiasl and I. M. Lewis, *Phys. Rev. D* **89**, 055026 (2014) [arXiv:1309.6640 [hep-ph]].
- [42] Y. Hochberg, E. Kuflik, H. Murayama, T. Volansky and J. G. Wacker, arXiv:1411.3727 [hep-ph].
- [43] Y. Hochberg, E. Kuflik, T. Volansky and J. G. Wacker, *Phys. Rev. Lett.* **113**, 171301 (2014) [arXiv:1402.5143 [hep-ph]].
- [44] N. Yamanaka, S. Fujibayashi, S. Gongyo and H. Iida, arXiv:1411.2172 [hep-ph].
- [45] X. W. Liu, X. F. Wu and T. Lu, arXiv:0808.1172 [astro-ph].
- [46] P. H. Frampton and B. H. Lee, *Phys. Rev. Lett.* **64**, 619 (1990).
- [47] T. Hambye, *JHEP* **0901**, 028 (2009) [arXiv:0811.0172 [hep-ph]].
- [48] T. W. B. Kibble, *Phys. Rept.* **67**, 183 (1980).
- [49] T. W. B. Kibble, *J. Phys. A* **9**, 1387 (1976).
- [50] Y. B. Zeldovich, I. Y. Kobzarev and L. B. Okun, *Zh. Eksp. Teor. Fiz.* **67**, 3 (1974) [*Sov. Phys. JETP* **40**, 1 (1974)].
- [51] M. Gonderinger, H. Lim and M. J. Ramsey-Musolf, *Phys. Rev. D* **86**, 043511 (2012) [arXiv:1202.1316 [hep-ph]].
- [52] V. Barger, P. Langacker, M. McCaskey, M. Ramsey-Musolf and G. Shaughnessy, *Phys. Rev. D* **79**, 015018 (2009) [arXiv:0811.0393 [hep-ph]].
- [53] A. Biswas, D. Majumdar, A. Sil and P. Bhattacharjee, *JCAP* **1312**, 049 (2013) [arXiv:1301.3668 [hep-ph]].

- [54] J. Edsjo and P. Gondolo, Phys. Rev. D **56**, 1879 (1997) [hep-ph/9704361].
- [55] K.A. Olive et al. (Particle Data Group), Chin. Phys. C, 38, 090001 (2014).
- [56] R. D. Young and A. W. Thomas, Phys. Rev. D **81**, 014503 (2010) [arXiv:0901.3310 [hep-lat]].
- [57] D. S. Akerib *et al.* [LUX Collaboration], Phys. Rev. Lett. **112**, no. 9, 091303 (2014) [arXiv:1310.8214 [astro-ph.CO]].
- [58] R. Barate *et al.* [LEP Working Group for Higgs boson searches and ALEPH and DELPHI and L3 and OPAL Collaborations], Phys. Lett. B **565**, 61 (2003) [hep-ex/0306033].
- [59] Z. Kang, J. Li, T. Li, D. Liu and J. Shu, Phys. Rev. D **88**, no. 1, 015006 (2013) [arXiv:1301.0453 [hep-ph]].
- [60] R. S. Chivukula, A. Farzinia, J. Ren and E. H. Simmons, Phys. Rev. D **88**, 075020 (2013) [arXiv:1307.1064 [hep-ph]].
- [61] R. Khosravi and F. Falahati, Phys. Rev. D **88**, no. 5, 056002 (2013).
- [62] G. Degrandi, S. Di Vita, J. Elias-Miro, J. R. Espinosa, G. F. Giudice, G. Isidori and A. Strumia, JHEP **1208**, 098 (2012) [arXiv:1205.6497 [hep-ph]].
- [63] J. Fleischer and F. Jegerlehner, Phys. Rev. D **23**, 2001 (1981).
- [64] A. Sirlin and R. Zucchini, Nucl. Phys. B **266**, 389 (1986).
- [65] M. J. G. Veltman, Acta Phys. Polon. B **12**, 437 (1981).
- [66] P. Gondolo and G. Gelmini, Nucl. Phys. B **360**, 145 (1991).
- [67] K. P. Modak, D. Majumdar and S. Rakshit, arXiv:1312.7488 [hep-ph].